Entropy Generation Rate for a Peristaltic Pump

Article *in* Journal of Non-Equilibrium Thermodynamics · June 2009

DOI: 10.1515/JNETDY.2009.010

CITATIONS
17

READS
131

3 authors, including:

Ferhat Souidi
University of Science and Technology Houari Boumediene
7 PUBLICATIONS **22** CITATIONS
SEE PROFILE

Benyahia Nabil
Université de Bouira
4 PUBLICATIONS **19** CITATIONS
SEE PROFILE

J. Non-Equilib. Thermodyn.
2009 · Vol. 34 · pp. 171–194

Entropy Generation Rate for a Peristaltic Pump

Ferhat Souidi*, Kheira Ayachi, and Nabil Benyahia
Faculté de Physique, Université des Sciences et de la Technologie,
Houari Boumediène, 16111 Bab Ezzouar, Algier, Algeria

*Corresponding author (sou_fer@yahoo.com)

Communicated by E.E. Michaelides, San Antonio, USA

Abstract

In view of the second law of thermodynamics, the idealized process is usually so selected as to be one of minimum available energy degradation. A measure of departure from this ideal process is the entropy generation rate. In this paper, we shall investigate this aspect concerning an adiabatic peristaltic pump. Our analysis also exhibits the general features of a flow in a contracting tube. It is shown that the dynamics of the system can be reduced to that of a classical Hagen-Poiseuille flow with a source term in the continuity equation and an additional induced force in the momentum equation.

In reference to exergy, the analysis reveals that peristaltic pumps generate more entropy than steady walled tubes and are not, from this point of view, competitive devices. The reason for this high-energy degradation is found in the dynamic behavior. The flow rate is not constant along the tube, but increases as sections downstream are reached. This results in high velocity gradients and therefore in strong dynamic irreversibility, which is the prime entropy source of the system. For the classical Hagen–Poiseuille flow, the entropy is mainly generated by heat diffusion.

1. Introduction

The environment protection problems and the concern about energy savings have recently motivated scientists to conduct analyses about the energy efficiencies of various industrial and energy-consuming facilities. The optimization of the operating conditions of these devices goes necessarily through the minimization of the entropy generation rate according to the second law of thermodynamics. This topic has occupied increasing attention in the past two

 DOI 10.1515/JNETDY.2009.010

decades and constitutes the subject of several publications and communications. Hereafter, we will summarize some of them.

Bejan [1, 2] presented the second law aspect of convection heat transfer. He introduced the concept of entropy generation number and irreversibility distribution ratio and presented entropy generation profiles for several configurations. Since then, numerous investigations have been performed for other flow situations and thermal boundary conditions. Mahmoud and Fraser [3] have investigated analytically the first and second law characteristics of fluid flow and heat transfer inside a channel having two parallel plates with a finite gap between them. The fluid is assumed to be non-Newtonian and follows the power law model. It has been reported that the axial conduction term has a negligible effect on the total entropy generation rate, which is significantly affected by the viscous dissipation, the Prandtl number, and the temperature difference. For a fluid index $n < 1$, maximum entropy generates at the center and then decreases. For fluids having $n > 1$, a second maximum of the Bejan number is observed inside the fluid region. These authors [4] conducted the same investigation for cylindrical Couette flow with isoflux thermal boundary conditions. They report that the entropy generation rate is higher near the inner cylinder due to the presence of sharp velocity gradients. The location of the minimum Bejan number shifts toward the outer cylinder as the velocity ratio increases. In a subsequent paper [5], they compare the entropy generation rate of a fluid flow inside a channel of circular cross section with that made of two parallel plates with the same gap. The fluid is non-Newtonian. Tasnim et al. [6] investigated the entropy generation rate in a porous vertical channel with hydro-magnetic effect and mixed convection flow. They report that both walls act as strong concentrator of irreversibility. They introduced a group parameter $\left(\psi = U_0^2 \mu T_0 / \Delta T^2 k\right)$ and showed that for $\psi = 0$, the fluid friction irreversibility becomes zero and the entropy generation number falls linearly toward the hot wall. For higher ψ ($\psi = 8$), fluid friction irreversibility dominates and the entropy generation number rapidly increases with transverse distance. Haddad et al. [7] studied the entropy generation due to laminar forced convection of a Newtonian fluid in the entrance region of a concentric annulus subject to different thermal boundary conditions. Entropy generation is inversely proportional to both Reynolds number and entrance temperature. They also show that increasing the Eckert number and/or the radius ratio will increase the entropy generation. Finally, they report that thermal entropy generation is relatively dominant over viscous entropy generation. Lingen Chen and coworkers [8] reexamined the historical background, and the state-of-the-art of finite time thermodynamic theory and its applications, from the point of view of both physics and engineering. The emphasis was on the performance optimization of thermodynamic processes and devices including heat engines and heat pumps and other processes. It is pointed out that the generalized op-

timization theory is the development direction of finite thermodynamics in the future. Michaelides and Michaelides [9] developed a new method for the determination of friction factors through the computation of irreversibility and entropy rate production. They extend the single fluid variable model to include the entropy production in multiphase systems. They show that in a two-phase system, the entropy dissipation is caused by two effects: the mechanical energy dissipation due to shear stresses and the hold-up effect due to the non-uniform density. The latter is responsible for the higher rates of dissipation observed in vertical pipe flows as compared with horizontal ones.

The literature review reveals that attention has so far focused on classical systems (Poiseuille, Couette, annulus. . .); yet the contemporary trend in the field of fluid flow tends toward systems with moving and/or deformable boundaries. This trend is mainly motivated by the desire of the fluid mechanics scientific community to contribute to viable solutions to problems dealing with biological fluid systems. For a comprehensive review on this topic, see Heil [10], Benyahia and Souidi [11], among others.

At variance with the dynamic problem, and to the knowledge of the authors, scant attention has been paid to the thermal and thermodynamic aspects of such systems. It is precisely the purpose of this article to highlight these aspects. We consider a contracting tube closed at the upstream end by an adiabatic valve, the content is propelled downstream, into the adjoining sections by the contraction of the wall. This phenomenon, called peristalsis, is particularly observed in the cardiovascular pump. In fact, during the systolic phase of the cardiovascular pump, the mitral valve is closed while the atrioventricular valve is open. At this stage the ventricle forms a vessel with one end closed.

Peristalsis pumping also has a possibility of engineering applications; it has been quite utilized for the transport of such fluids as slurries or corrosive fluids when it is desirable to prevent them from coming into contact with the mechanical parts of the pump [12]. Thus, the general analysis of this paper seems interesting from both the theoretical and applicative points of view.

2. Mathematical formulation

2.1. General specifications

Consider the flow of an incompressible viscous fluid, with density ρ, kinematic viscosity ν, and conductivity k, moving through an adiabatic tube with rectilinear axis and circular cross section of radius R_0 (t). The tube is closed at the upstream end by an adiabatic valve and extends far downstream. The

x-axis coincides with the tube axis and with the origin at the center of the valve. The model problem is illustrated in Figure 1.

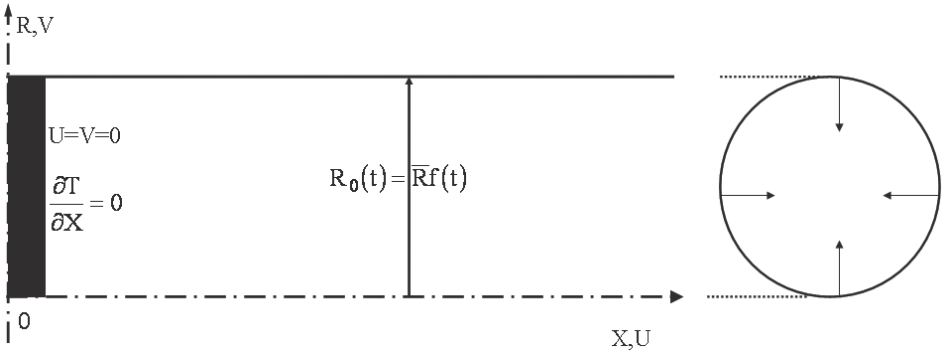

Figure 1 Sketch of the contracting tube.

The governing equations are (see Appendix A):

$$\frac{\partial(\eta u)}{\partial x}+\frac{\partial(\eta w)}{\partial \eta}=\Omega \tag{1a}$$

$$\frac{\partial u}{\partial \tau}+u\frac{\partial u}{\partial x}+w\frac{\partial u}{\partial \eta}=-\frac{\partial p}{\partial x}+\frac{1}{Re}\frac{1}{\eta}\frac{\partial}{\partial \eta}\left(\eta\frac{\partial u}{\partial \eta}\right)+F \tag{1b}$$

$$\frac{\partial p}{\partial \eta}=0 \tag{1c}$$

$$\Omega=\eta(1-f)\frac{\partial u}{\partial x}-\frac{\partial f}{\partial \tau} \tag{1d}$$

$$F=\frac{1-f^2}{f^2}\frac{1}{Re}\frac{1}{\eta}\frac{\partial}{\partial \eta}\left(\eta\frac{\partial u}{\partial \eta}\right)+\frac{f-1}{f}w\frac{\partial u}{\partial \eta}+(\eta-1)\frac{1}{f}\frac{\partial f}{\partial \tau}\frac{\partial u}{\partial \eta} \tag{1e}$$

$$\left.\begin{aligned} &u(x,1,\tau)=u(0,\eta,\tau)=w(x,1,\tau)=\left.\frac{\partial u}{\partial \eta}\right|_{\eta=0}=p(0,\tau)=0\\ &u(x,\eta,0)=-2x\frac{1}{f}\left.\frac{\partial f}{\partial \tau}\right|_{\tau=0}\end{aligned}\right\} \tag{1f}$$

The model solves the flow problem by recasting the governing equations into the standard Hagen–Poiseuille form. An additional induced force F in the

momentum equation, and a source term Ω in the continuity equation, account for movement of the wall. To close the problem, we introduce the integral form of the continuity equation (see Appendix A):

$$\int_0^1 u(x, \eta, \tau)\, \eta d\eta = \frac{\left|f'(\tau)\right|}{f(\tau)} x \tag{2}$$

In terms of the physical variables, the energy equation is given by:

$$\left.\begin{aligned} &\frac{\partial \theta}{\partial \tau} + u\frac{\partial \theta}{\partial x} + w\frac{\partial \theta}{\partial r} = \frac{1}{Pe}\frac{1}{r}\frac{\partial}{\partial r}\left(r\frac{\partial \theta}{\partial r}\right) + \frac{E_c}{Re}\varphi \\ &\theta(x, r, 0) = 1; \quad \left.\frac{\partial \theta}{\partial x}\right|_{x=0} = \left.\frac{\partial \theta}{\partial r}\right|_{r=0} = 0 \\ &\left.\frac{\partial \theta}{\partial r}\right|_{r=r_0(\tau)} + Bi.\theta_w = 0 \end{aligned}\right\} \tag{3}$$

2.2. Entropy generation rate

The entropy generation rate is partitioned into two components, heat diffusion and viscous dissipation. In the entropy representation, it is given by

$$S = \vec{\nabla}\left(\frac{1}{T}\right)\left(-k\vec{\nabla}T\right) + \frac{\mu}{T}\Phi = k\left(\frac{\vec{\nabla}T}{T}\right)^2 + \frac{\mu}{T}\Phi.$$

The first term measures the thermal energy degradation as heat diffuses from high to low temperature regions; the second term gives the "destroyed" mechanical energy as kinetic energy is transformed into heat by viscous dissipation.

Its dimensionless version is

$$s = \frac{S}{S_k + S_\mu} = \frac{1}{1 + Ec.Pr}\left(\frac{1}{\theta + \omega}\right)^2\left[\left(\frac{\partial \theta}{\partial r}\right)^2 + \left(\frac{\partial \theta}{\partial x}\right)^2\right] + \frac{Ec.Pr}{1 + Ec.Pr}\left(\frac{\varphi}{\theta + \omega}\right) \tag{4}$$

S_k and S_μ are the diffusion and dissipation scaling parameters given by $S_k = \frac{k}{R^2}$ and $S_\mu = \frac{\mu}{\Delta T}\left(\frac{V_0}{R}\right)^2$, respectively. $\omega = \frac{T_\infty}{T_0 - T_\infty}$ measures the temperature difference.

Finally, we introduce the Bejan number,

$$Bj\,(x, \eta, \tau) = \frac{k\left(\frac{\vec{\nabla} T}{T}\right)^2}{k\left(\frac{\vec{\nabla} T}{T}\right)^2 + \frac{\mu}{T}\Phi}. \tag{5}$$

It gives the part of the entropy rate generated by heat diffusion.

3. Numerical analysis

We develop a special code to solve numerically the governing equations. It is based on an implicit finite difference scheme. The inertia term is linearized through a Taylor series expansion around the previous time step. The velocity and temperature profiles being expected to be very steep near the wall, a non-uniform grid, tight near $\eta = 1$, is considered. The coordinates (x, η) of the nodal point (i,j) are given by

$$x = (i-1)\,\Delta x; \quad \eta = \left(1 - \left(\frac{J-(j-1)}{J}\right)^{\varepsilon}\right)$$
$$1 \le i \le I+1, \quad 1 \le j \le J+1.$$

I and J are the total number of nodal points in the x and η directions, respectively; ε is the grid coefficient. In order to respect the second-order precision, a four-nodal point discretization for the second-order derivative and a three-nodal point for the first order are performed. We finally use the Gaussian elimination with partial pivoting method to solve the linear algebraic equation systems. To ensure grid-insensitive results, we conducted computations for several values for J and ε. For J greater than 120, no appreciable changes were noticed. As for the grid coefficient, the value of $\varepsilon = 3$ was retained. The time step is chosen to both guarantee stability conditions and avoid excessive computation time. The optimal time step is 2.10^{-3}. Concerning stability, we recall that, the numerical scheme being fully implicit, it is unconditionally stable provided no reversed flow is present in the field. Indeed, during the calculation procedure, no instability due to unlimited growth of the round-off error was ever detected. The number of iterations within each time step increases with time, though within reasonable limits (from 8 iterations for the first time steps to 15 for the last ones with no under-relaxation factor). As to consistency and convergence, we shall rely on validation and mass conservation tests.

We turn now to the computation procedure. Equations (1a) and (2) are two different forms of the same continuity equation and should not be solved simultaneously. For x and τ fixed, we estimate the radial component of the velocity profile w, then use Eqs. (1b)–(2) to calculate the axial velocity component and the pressure. Equation (1a) gives the new value of the radial component, which is compared to the previous one. We iterate until convergence. Meanwhile, we check both the flow rate as we progress downstream and the convergence rate of the velocity field. Once the velocity field has been obtained, we proceed to determine from Eq. (3) the temperature field in the physical coordinate system (x, r, τ) and, finally, the entropy generation rate from Eq. (4).

4. Validation

The chief aim in this section is to assess the adequacy of the flow model.

Uchida and Aoki [13] propose an exact solution of the Navier–Stokes equations for unsteady flow in a semi-infinite contracting pipe. A full solution, similar in both space and time, is obtained provided the radius of the pipe varies in time as

$$R_0(t) = \overline{R} f(t) = \overline{R}\sqrt{1 - \alpha t}.$$

We retain this expression in what follows.

4.1. Code validation and mass conservation tests

The code is validated by performing a number of tests.

In Figure 2a, the streamlines obtained in the present study are compared with those given by Uchida and Aoki [13]. We note an excellent agreement between the analytical and numerical solutions. Figure 2b compares the flow rate as given by the numerical model $q(x, \tau) = 2\pi f^2 \int_0^1 u(x, \eta, \tau)\eta d\eta$ (Simpson integral adapted to a non-uniform grid), with that given by the theoretical formulation $q(x, \tau) = 2\pi f \left|\frac{df}{d\tau}\right| x = \pi |\alpha x|$ (Appendix A).

The numerical results and the analytical solution coincide perfectly. These two tests give great confidence in both, the model and the specific numerical code.

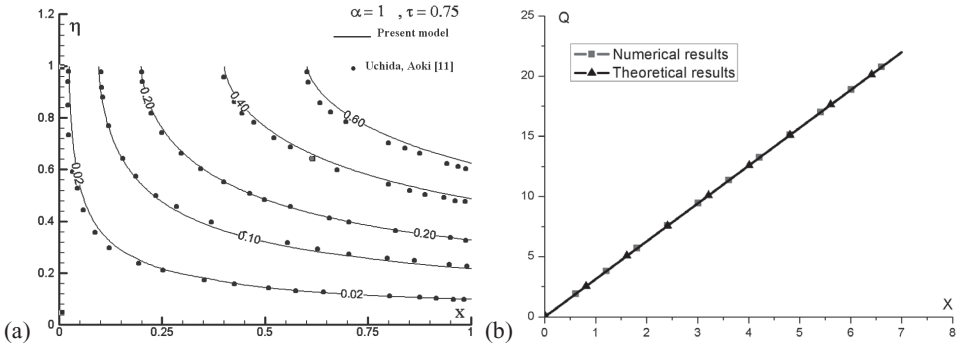

Figure 2 (a) Streamlines for a contracting tube; (b) flow rate versus axial position.

5. Dynamic problem

5.1. Source term and velocity components

Figure 3a,b gives the axial and radial velocity profiles at various axial locations. The axial component presents the parabolic aspect of the Hagen–Poiseuille flow with a linear increase along the axis. Concerning the radial component, it is x invariant as predicted by the mathematical formulation and contains an important physical concept, viz. the displacement thickness. To compensate for the flow retardation caused by strong friction forces, the transverse velocity increases in the near wall viscous region. Consequently, the streamlines are displaced by a distance known in boundary layer theory as the displacement thickness. On the axis, the transverse velocity component falls to zero to meet the axially symmetrical flow configuration.

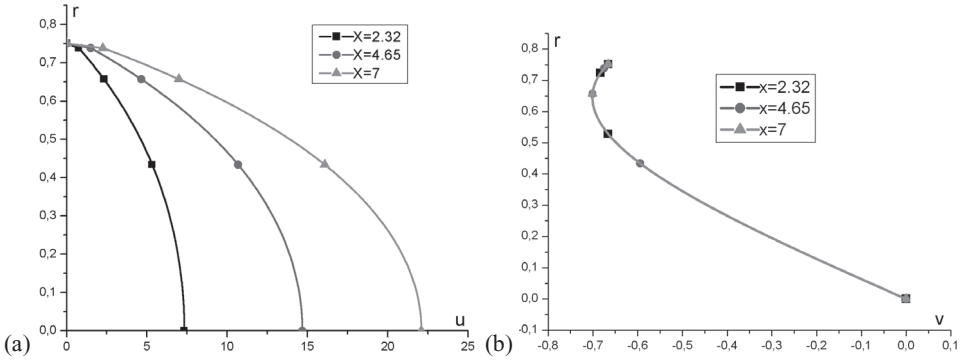

Figure 3 (a) Axial velocity profiles; (b) radial velocity profiles.

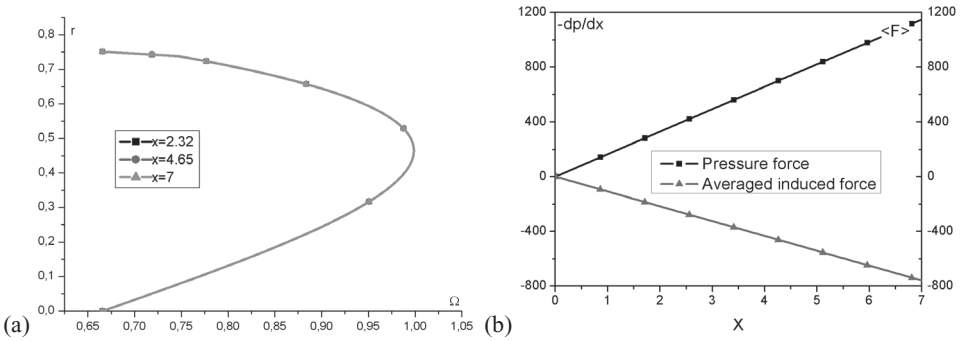

Figure 4 (a) Profiles of Ω at three different axial locations; (b) averaged pressure force and induced force F along the axis.

In Figure 4a, we report the profiles of the source Ω at three different positions along the axis. We note that it is independent of the axial position x in conformity with Eq. (1d). These results are in perfect agreement with the linear increase of the flow rate, as reported above (Appendix A).

Figure 4b reveals that the magnitude of the mean induced force increases linearly with the axial position x and opposes the accelerating pressure force. At this stage, it might be convenient to comment upon the action of the wall on the dynamics of the flow. The contraction of the tube results in a linear increase of the fluid velocity u and velocity gradient $\frac{\partial u}{\partial r}$ as we progress downstream, i.e., an increase in the inertia and viscous forces, respectively. These additional forces are precisely what the induced force F expresses.

5.2. Steady case

In order to examine the effects of peristalsis on the entropy generation rate, we shall consider the classical Hagen–Poiseuille flow case regarded as a reference state. The results are compared with those obtained for the contracting tube.

6. First and second law of thermodynamics

We present and analyze on physical grounds a selected set of graphical results. The set includes, in addition to temperature profiles, the entropy rate averaged over the cross section:

$$\langle s(x, \tau_0)\rangle = 2\int_0^1 s(x, \eta, \tau_0)\,\eta d\eta, \tag{6}$$

the integrated entropy generation rate:

$$\langle\langle s(\tau_0)\rangle\rangle = 2\int_0^{x_m}\left(\int_0^1 s(x,\eta,\tau_0)\,\eta d\eta\right)dx, \tag{7}$$

the mean Bejan number:

$$\langle Bj(x,\eta,\tau)\rangle = \frac{\langle k\left(\frac{\vec{\nabla}T}{T}\right)^2\rangle}{\langle k\left(\frac{\vec{\nabla}T}{T}\right)^2 + \frac{\mu}{T}\Phi\rangle}. \tag{8}$$

The computations are performed for $\omega = 50$. The profiles are plotted at $x = x_m/3$ and $\tau_0 = 0.437$ corresponding to $f = 0.75$.

6.1. Effects of the Biot number (Bi)

The Biot number regulates the heat exchange with the reservoir at T_∞. It affects a thin near-wall region where viscous dissipation is the most effective. We analyze the effects for intermediate values of Eckert, Prandtl, and Reynolds numbers: $Ec = 0.1$, $Pr = 7$, $Re = 50$.

A closer examination of the thermal wall boundary condition, Eq. (3), reveals that for small values of Bi, the wall acts as an adiabatic surface, the fluid and wall temperatures rise in response to the heat generated by viscous dissipation. For large Bi, the system loses more heat to the cooler surroundings, maintaining the temperature of the fluid and that of the wall at a relatively low level. For $Bi = 10^2$, the thermal resistance $1/h_\infty$ is low and the wall assumes the temperature of the surroundings: ($\theta_w = 0$). These results are reported in Figure 5a. Owing to the value of Pr, heat penetration does not reach the centerline where the fluid maintains its initial temperature ($\theta_0 = 1$).

Figure 5b depicts the evolution along the axis of the mean fluid temperature (mixing cup temperature) with Bi as a parameter. As expected, the curves exhibit a parabolic aspect with respect to x. Increasing Bi results in more heat leaving the system and then to lower fluid and wall temperatures.

The evolution along the axis of the entropy generation rate averaged over the cross section is given in Figure 5c. Large values of Bi result in a greater entropy generation rate owing to a larger temperature gradient at the wall and lower fluid temperature. For smaller values of Bi, heat is hardly evacuated and

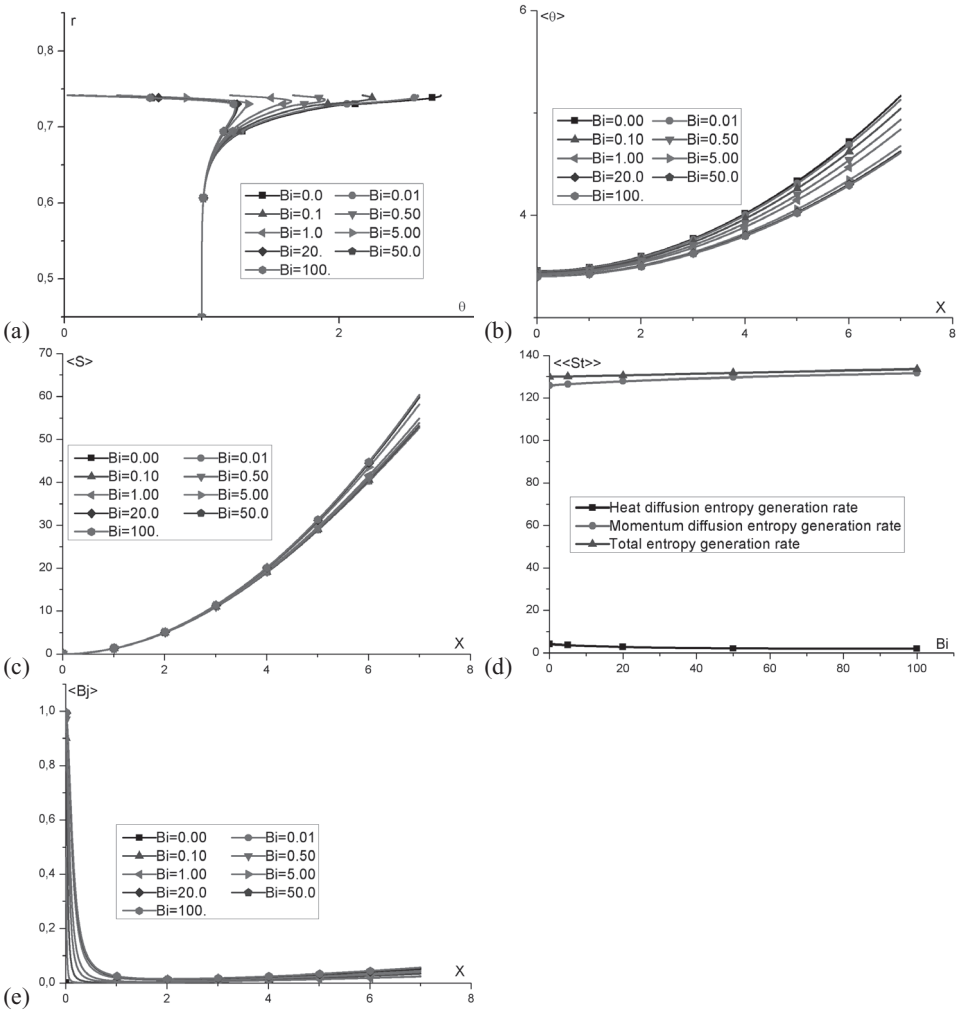

Figure 5 (a) Temperature profiles for different values of Bi; (b) mixing cup temperature versus x for different values of Bi; (c) averaged entropy generation rate versus x for different values of Bi; (d) volumetric entropy generation rate versus Bi; (e) averaged Bejan number versus x for different values of Bi.

maintains the fluid temperature at a sufficiently high level to keep the entropy generation rate relatively low.

Going back to Eq. (4), we note that for $\omega \gg \theta$, with $\omega = 50$, $\theta \leq 3$, the dynamic component of the entropy generation rate, which is the major component, varies like φ, i.e., like x^2. This is illustrated by the quadratic aspect of the curves.

Figure 5d gives the evolution of the integrated entropy generation rate versus Bi. It indicates that the major component of the entropy generation rate is the dynamic component as stated above. An increase in Bi results in two antagonistic effects: on the one hand, the entropy rate increases due to lower fluid temperature and, on the other hand, the region of entropy production, i.e., sharp temperature gradient, shrinks. These two effects inhibit each other, resulting in an integrated averaged entropy generation rate almost insensitive to Bi.

Figure 5e presents the evolution of the averaged Bejan number along the axis. In the vicinity of the valve, the flow rate is low and entropy is affected only by heat diffusion: for large Bi, $\langle \mathrm{Bj} \rangle$ approaches 1. Downstream, the flow rate builds up and momentum diffusion becomes the main entropy source resulting in $\langle \mathrm{Bj} \rangle$ approaching zero.

In subsequent analysis, we shall consider an isolated system ($\mathrm{Bi} = 0$), so only internal irreversibilities due to heat and momentum diffusion within the fluid are of interest.

6.2. Effects of the Reynolds number

The Reynolds number affects principally the dynamics of the flow. We analyze its impact on the system for water ($\mathrm{Pr} = 7$) and moderate viscous dissipation: ($\mathrm{Ec} = 0.1$).

Figure 6a compares the temperature profiles for different values of Re.

The heat source term in the energy equation is governed by the parameter Ec/Re. As Re increases, a larger amount of heat generated by viscous dissipation in the near wall region is convected downstream, resulting hence in lower local fluid and wall temperatures. Meanwhile, as Re increases for fixed Pr, the thickness of the entropy region (sharp temperature gradient), depending on the Peclet number, gets thinner. Near the axis, no viscous dissipation is present and the temperature remains unchanged

In Figure 6b, we report the volumetric entropy generation rates versus Re. It indicates that the major component of entropy generation rate is the dynamic component. It increases with Re, owing to both an increase in the velocity gradient near the wall and a lower fluid temperature level. As to the heat entropy generation rate, it is controlled by both temperature and temperature gradient with opposite effects. For small values of Re ($\mathrm{Re} < 100$), the temperature is the determining factor. An increase in Re reduces the temperature of the fluid and results in larger entropy generation. In the range of large Re,

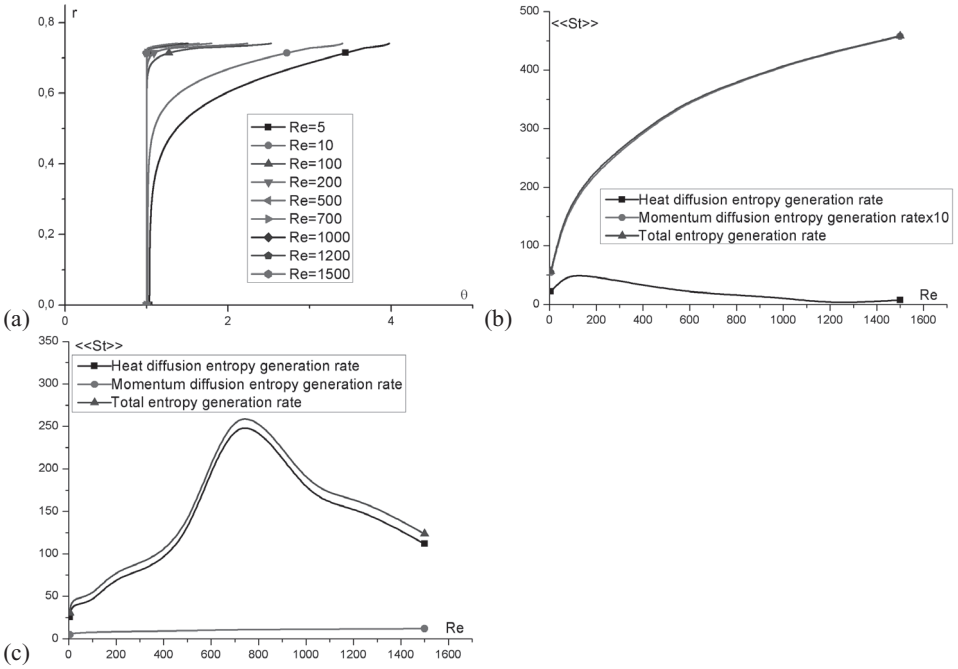

Figure 6 (a) Temperature profiles for different values of Re; (b) volumetric entropy generation rates versus Re; (c) volumetric entropy generation rates versus Re (steady case).

the temperature remains unchanged over nearly the entire field ($\theta = 1$ for all $\mathrm{Re} > 100$) and is no longer the influencing factor.

As Re increases, regions of sharp temperature gradient (region of entropy production) narrow and result in decreasing integrated entropy generation rate.

To grasp the effect of a wall's movement on entropy generation, we turn to the stationary case. Figure 6c reports the volumetric entropy generation rates.

At variance with the unsteady case, the heat diffusion is the mean entropy generation component. The figure reveals that maximum entropy generates at intermediate values of Re ($700 < \mathrm{Re} < 1000$). The observations described above for the unsteady case hold for this stationary case. At low Re, the relative high fluid temperature maintains the entropy generation rate at a low level; at the other limit, the effects of the gradients take place and result in less entropy generation as Re increases. Finally, the analysis reveals that peristalsis is a great entropy generator process and this is due essentially to dynamic irreversibilities.

6.3. Effects of the Prandtl number (Pr)

The Prandtl number characterizes the fluid. It is the ratio of the momentum diffusion coefficient over the thermal diffusion coefficient. We analyze its effects for $Ec = 0.1$, $Re = 50$.

Figure 7a shows the fluid temperature profiles with Pr as a parameter.

For small Pr ($Pr < 0.1$) the thermal diffusion coefficient ($k/\rho c$) is large and heat generated by viscous dissipation near the wall diffuses through the fluid and reaches the centerline, where the temperature increases slightly. This results in nearly uniform temperature profiles. For large values of Pr, the thermal resistance $\left(\overline{R}/k\right)$ is strong enough to prevent heat from diffusing through the fluid. We observe a sharp increase in the temperature near the wall, where velocity gradients and then dissipation function are significant. The centerline temperature remains unchanged. We note also that the wall temperature increases continuously with Pr.

In Figure 7b, the volumetric entropy generation rates are plotted against Pr. The figure shows that thermal irreversibility increases with Pr up to $Pr \approx 10$, then decreases due to higher temperatures near the wall. Dynamic

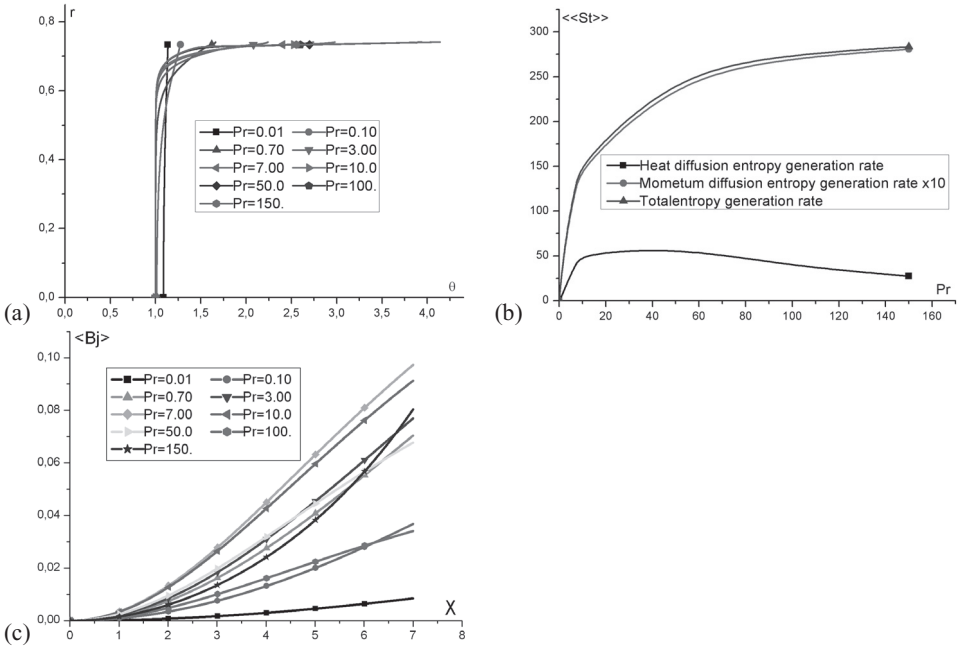

Figure 7 (a) Temperature profiles for different values of Pr; (b) volumetric entropy generation rates versus Pr; (c) averaged Bejan number versus x for different values of Pr.

irreversibility is an increasing monotonic function of Pr, owing to the coefficient $\Pr \cdot \mathrm{Ec}/1 + \Pr \cdot \mathrm{Ec}$, principally at low Pr where we observe a sharp increase. It is the determinant entropy source. These results are confirmed by the behavior of the averaged Bejan number as given in Figure 7c.

For all Pr, $\langle \mathrm{Bj} \rangle$ is less than 1 and reveals that the major component in entropy generation is the dynamic component.

6.4. Effects of the Eckert number (Ec)

Eckert number is a measure of the kinetic energy transformed into heat by viscous dissipation. We analyze its effects for intermediate value of the Prandtl number: $\Pr = 7$ (water), $\mathrm{Re} = 50$.

Figure 8a displays the temperature profiles with the Eckert number as a parameter.

For small Ec, no heat source is present within the system. The fluid maintains its initial temperature all through ($\theta = 1$). For large Ec, kinetic energy is transformed into heat and we observe a substantial temperature rise as we approach the wall where velocity gradient develops. The heat generated there does not diffuse up to the axis in view of the value of Pr. In Figure 8b, we report the volumetric entropy generation rates versus Ec. We notice that the temperature effect overcomes the amplifying effect of the temperature gradient for large values of Ec. In this region, the fluid temperature increases with Ec and results in a smaller entropy generation rate. In the other limit, the factor

$$\frac{\mathrm{Ec} \cdot \Pr}{1 + \mathrm{Ec} \cdot \Pr}$$

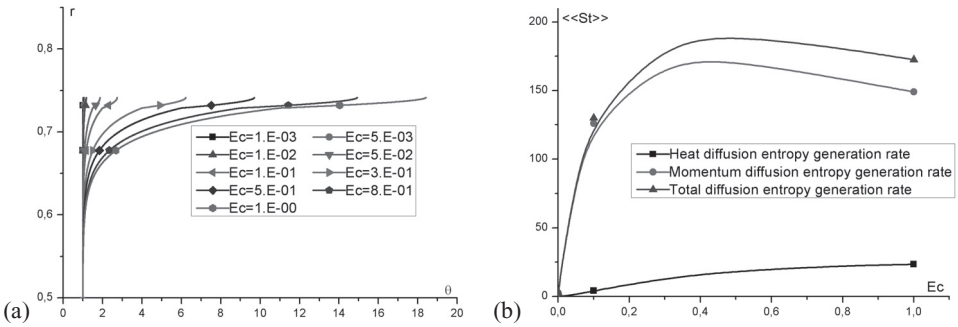

Figure 8 (a) Temperature profiles for different values of Ec; (b) volumetric entropy generation rates versus Ec.

is most important and we observe an increase of the entropy generation rate with Ec. Finally, we note that dynamic irreversibility is the main entropy source.

7. Conclusion

In addition to analyzing the energy degradation in a peristaltic pump, the present study exhibits the general features of a fluid flow in a contracting tube. Several interesting conclusions are drawn:

The flow is with a unique and major velocity component and obeys the boundary layer equations. The system reduces to the classical Hagen–Poiseuille flow with a source term in the continuity equation and an additional induced force in the momentum equation that account for the movement of the wall. The former results in a linear increase of the flow rate as sections downstream are reached; the latter tends to decelerate the flow through the inertia and viscous components.

In order to predict which parameters are critical for determining the quality of a peristaltic pump, various numerical results have been presented and analyzed. The study reveals that the heat exchange at the wall (Bi) does not influence greatly the exergy of the system, contrary to the dynamics of the flow (Re) and/or the type of fluid (Pr). It reveals also that peristaltic pumps generate more entropy than steady walled tubes and are not competitive devices from an exergetic efficiency standpoint. In these systems, the fluid carries "low-quality" energy. The reason for this high-energy degradation is found in the dynamic behavior. As mentioned above, the flow rate is not constant along the tube, but increases as sections downstream are reached and leads to extremely high velocity and velocity gradients and therefore to strong dynamic irreversibility, which is the prime entropy source of the system. For the classical Hagen–Poiseuille flow, the entropy is mainly generated by heat diffusion.

Nomenclature

Capital letters

Bi = Biot number: $\mathrm{Bi} = \frac{h_\infty \overline{R}}{k}$

Bj = Bejan number: $\mathrm{Bj}\,(x, \eta, \tau) = \frac{k\left(\frac{1}{T}\frac{\partial T}{\partial R}\right)^2}{k\left(\frac{1}{T}\frac{\partial T}{\partial R}\right)^2 + \frac{\mu}{T}\left(\frac{\partial U}{\partial R}\right)^2}$

Ec = Eckert number: $\mathrm{Ec} = \frac{V_0^2}{c(T_0 - T_\infty)}$

F = Dimensionless induced force

P = Fluid pressure

P_0 = inlet fluid pressure

Pr = Prandtl number: $\Pr = \frac{\mu c}{k}$

Pe = Peclet number: $\mathrm{Pe} = \mathrm{Re}.\,\Pr$

Q = Volumetric flow rate: $Q(X) = 2\pi R_0(t)\left|\frac{dR_0}{dt}\right| X.$

R = Radial coordinate

$\overline{R}$ = Initial radius of the tube

Re = Reynolds number: $\mathrm{Re} = \frac{\overline{R}^2}{\alpha^{-1}\nu} = \left(\frac{\overline{R}}{\delta\mu}\right)^2$

R_0 = Instantaneous radius of the tube: $R_0(t) = \overline{R}\sqrt{1-\alpha t}$

S = Entropy generation rate

S_μ = Entropy scaling parameter (viscous dissipation): $S_\mu = \frac{\mu}{\Delta T}\left(\frac{U_0}{\overline{R}}\right)^2$

S_k = Entropy scaling parameter (heat diffusion): $S_k = \frac{k}{\overline{R}^2}$

T = Fluid temperature

T_0 = Initial fluid temperature

T_∞= Temperature of the surroundings

U = Axial velocity

V= Radial velocity

V_0 = Characteristic velocity: $V_0 = \alpha\overline{R}$

X = Axial coordinate

X_m = Tube's length

Lower case letters

c = Specific heat

f = Dimensionless tube radius; f= $\sqrt{1-\alpha t}$

h_∞ = Heat convection coefficient

k = Thermal conductivity

p = Dimensionless pressure: $p = \frac{P_0 - P}{\rho V_0^2}$

q = Dimensionless flow rate

r = Dimensionless radial coordinate: $r = \frac{R}{R}$

s = Dimensionless entropy generation rate

u = Dimensionless axial velocity

v = Dimensionless radial velocity

w = Radial velocity :$w = v - {}^{\partial f}/_{\partial \tau}$

x = Dimensionless axial coordinate

x_m= Dimensionless tube's length

Δx = Uniform step size in the axial direction

Greek letters

α = Peristalsis strength

δ_μ = Dynamic boundary layer thickness

δ_θ = Thermal boundary layer thickness

ε = Grid coefficient

η = Stretched radial coordinate: $\eta = \frac{R}{R_0(t)} = \frac{r}{f(\tau)}$

θ = Dimensionless fluid temperature

θ_w = Dimensionless wall temperature

μ =Dynamic viscosity

ν = Kinematic viscosity

ρ = Fluid density

τ = Dimensionless time, $\tau = \alpha t$

ω =Temperature parameter: $\omega = \frac{T_\infty}{T_0 - T_\infty}$

$\Omega =$ Source term (continuity equation)

$\Phi =$ Dimensional dissipation function

$\varphi =$ Dimensionless dissipation function:

$$\varphi = \left(\tfrac{\partial u}{\partial r}\right)^2 + 2\left[\left(\tfrac{v}{r}\right)^2 + \left(\tfrac{\partial v}{\partial r}\right)^2 + \left(\tfrac{\partial u}{\partial x}\right)^2\right]$$

Symbols

$\langle \quad \rangle$ Average over cross section: $\langle(\,)\rangle = \dfrac{2\pi \int_0^{R_0(t)} (\,)R\,dR}{\pi R_0^2(t)} = 2\int_0^1 (\,)\,\eta\,d\eta$

$\langle\langle(\,)\rangle\rangle =$ Average over volume: $\langle\langle(\,)\rangle\rangle = \dfrac{2\pi \int_0^{R_0(t)} \int_0^{X_m} (\,)R\,dR\,dX}{\pi R_0^2(t) X_m} = 2\int_0^{x_m}\left[\int_0^1 (\,)\,\eta\,d\eta\right]dx$

Appendix A

The classical axisymmetric cylindrical Navier–Stokes equations for a viscous incompressible fluid read:

$$\left.\begin{aligned}
&\frac{\partial (RU)}{\partial X} + \frac{\partial (RV)}{\partial R} = 0\\
&\frac{\partial U}{\partial t} + U\frac{\partial U}{\partial X} + V\frac{\partial U}{\partial R} = -\frac{1}{\rho}\frac{\partial P}{\partial X} + \nu\nabla^2 U\\
&\frac{\partial V}{\partial t} + U\frac{\partial V}{\partial X} + V\frac{\partial V}{\partial R} = -\frac{1}{\rho}\frac{\partial P}{\partial R} + \nu\nabla^2 V\\
&\frac{\partial T}{\partial t} + U\frac{\partial T}{\partial X} + V\frac{\partial T}{\partial R} = \frac{k}{\rho c}\nabla^2 T + \frac{\Phi}{\rho c}\\
&\nabla^2 = \frac{\partial^2}{\partial X^2} + \frac{1}{R}\frac{\partial}{\partial R}\left(R\frac{\partial}{\partial R}\right)\\
&\Phi = \left(\frac{\partial U}{\partial R}\right)^2 + 2\left[\left(\frac{\partial U}{\partial X}\right)^2 + \left(\frac{\partial V}{\partial R}\right)^2 + \left(\frac{V}{R}\right)^2\right]
\end{aligned}\right\} \qquad \text{(A1)}$$

We formulate the problem in dimensionless terms by scaling the dependent and independent variables with the following reference quantities: $\overline{R} \equiv$ initial tube's radius; $V_0 \equiv$ initial wall velocity; $\overline{t} = \overline{R}V_0^{-1}$.

The dimensionless variables are then:

$$r = \frac{R}{\overline{R}},\quad x = \frac{X}{\overline{R}},\quad \tau = \frac{t}{\bar{t}},\quad u = \frac{U}{V_0},\quad v = \frac{V}{V_0}.$$

Likewise, we consider the dimensionless pressure and temperature: $p = \frac{P-P_0}{\rho V_0^2}$, $\theta = \frac{T-T_\infty}{T_0-T_\infty}$, with P_0 being the inlet pressure and T_0 the initial temperature; T_∞ is the ambient temperature.

Equation (A1) reduces then to:

$$\left.\begin{aligned}
&\frac{\partial (ru)}{\partial x} + \frac{\partial (rv)}{\partial r} = 0\\
&\frac{\partial u}{\partial \tau} + u\frac{\partial u}{\partial x} + v\frac{\partial u}{\partial r} = -\frac{\partial p}{\partial x} + \frac{1}{Re}\nabla^2 u\\
&\frac{\partial v}{\partial \tau} + u\frac{\partial v}{\partial x} + v\frac{\partial v}{\partial r} = -\frac{\partial p}{\partial r} + \frac{1}{Re}\nabla^2 v\\
&\frac{\partial \theta}{\partial \tau} + u\frac{\partial \theta}{\partial x} + v\frac{\partial \theta}{\partial r} = +\frac{1}{Re\,Pr}\nabla^2\theta + \frac{Ec}{Re}\varphi\\
&\nabla^2 = \frac{\partial^2}{\partial x^2} + \frac{1}{r}\frac{\partial}{\partial r}\left(r\frac{\partial}{\partial r}\right)\\
&\varphi = \left(\frac{\partial u}{\partial r}\right)^2 + 2\left[\left(\frac{\partial u}{\partial x}\right)^2 + \left(\frac{\partial v}{\partial r}\right)^2 + \left(\frac{v}{r}\right)^2\right]
\end{aligned}\right\} \qquad \text{(A2)}$$

where Re and Pr are the classical Reynolds and Prandtl numbers; Ec is the Eckert number.

The volume flow rate past a section x is supplied by the fluid which was contained in the now diminished volume of pipe between x = 0 and x, i.e., $q(x,\tau) = \frac{Q(x,\tau)}{V_0\overline{R}^2} = 2\pi \int_0^{r_0(\tau)} u(x,r,\tau)\,r\,dr = 2\pi r_0(\tau)\left|\frac{dr_0(\tau)}{d\tau}\right| x$, from which we deduce the integral form of the continuity equation:

$$\int_0^{r_0(\tau)} u(x,r,\tau) r.dr = r_0(\tau)\left|\frac{dr_0(\tau)}{d\tau}\right| x$$

The dimensionless mean flow velocity is given by

$$\langle u(x,\tau)\rangle = \frac{q(x,\tau)}{\pi r_0^2(\tau)} = 2x\frac{1}{r_0(\tau)}\left|\frac{dr_0(\tau)}{d\tau}\right|, \qquad \text{(A3)}$$

and indicates that the axial velocity component is proportional to x. As to the radial component, it can be easily seen from the continuity equation and the wall velocity that it is x invariant. These results simplify greatly the governing equations.

If $u(r, t, x) = \overline{u}(r, t)\, x$ and $v(r, t) = \overline{v}(r, t)$, Eq. (A2) becomes

$$\begin{cases} r\overline{u}(r,\tau) + \dfrac{\partial\left(r\overline{v}(r,\tau)\right)}{\partial r} = 0 \\ \dfrac{\partial\overline{u}}{\partial\tau}x + \overline{u}^2 x + \overline{v}\dfrac{\partial\overline{u}}{\partial r}x = -\dfrac{\partial p}{\partial x} + \dfrac{1}{Re}\dfrac{1}{r}\dfrac{\partial}{\partial r}\left(r\dfrac{\partial\overline{u}}{\partial r}\right)x \\ \dfrac{\partial\overline{v}}{\partial\tau} + \overline{v}\dfrac{\partial\overline{v}}{\partial r} - \dfrac{1}{Re}\dfrac{1}{r}\dfrac{\partial}{\partial r}\left(r\dfrac{\partial\overline{v}}{\partial r}\right) = -\dfrac{\partial p}{\partial r} \end{cases} \tag{A4}$$

From the x momentum equation, we deduce that the pressure force in the axial direction is a linear function of x:

$$\frac{\partial p}{\partial x} = A(r,\tau)\, x \quad \text{or} \quad p(x, r, \tau) = \frac{1}{2}A(r,\tau)\, x^2 + B(r,\tau),$$

with $B(r,\tau) = 0$ to meet the inlet pressure boundary condition. As to the radial momentum equation, we notice that both its left- and right-hand sides depend on different sets of independent variables and are necessarily equal to a constant. The constant is zero to meet the pressure condition on the axis $\left(\frac{\partial p}{\partial r}\Big|_{r=0} = 0\right)$. The radial momentum equation reduces then to $\frac{\partial p}{\partial r} = 0$, which is simply the main characteristic of a boundary layer type flow. The solutions of this model are exact in the sense that no approximations were needed to simplify the full elliptic equations to their reduced boundary layer form. The flow presents a principal direction in which convective transport is dominant.

Next, assuming that the axial heat diffusion is negligibly small as compared with the radial diffusion (large Peclet number), the energy equation reduces to

$$\frac{\partial\theta}{\partial\tau} + u\frac{\partial\theta}{\partial x} + v\frac{\partial\theta}{\partial r} = \frac{1}{Pe}\frac{1}{r}\frac{\partial}{\partial r}\left(r\frac{\partial\theta}{\partial r}\right) + \frac{Ec}{Re}\varphi \tag{A5}$$

and reveals that the temperature field is a quadratic function of x (recall that $\varphi \approx x^2$).

Finally, we express the radius of the tube as $R_0(t) = \overline{R} f(\tau)$ and introduce the independent stretched variable $\eta = \frac{R}{R_0(\tau)} = \frac{R}{\overline{R} f(\tau)} = \frac{r}{f(\tau)}$ along with the radial velocity $w = v - \frac{df}{d\tau}$. We use the composite derivatives rule,

$$\frac{\partial}{\partial \tau} = \frac{\partial}{\partial \tau} - \frac{1}{f}\frac{df}{d\tau}\frac{\partial}{\partial \eta}, \quad \frac{\partial}{\partial x} = \frac{\partial}{\partial x}, \quad \frac{\partial}{\partial r} = \frac{1}{f}\frac{\partial}{\partial \eta}, \quad \frac{\partial^2}{\partial r^2} = \frac{1}{f^2}\frac{\partial^2}{\partial \eta^2},$$

and express the governing equations in the new coordinate system (x, r, τ)

A. Continuity equation:

$$\text{*Differential form:} \quad f\frac{\partial(\eta u)}{\partial x} + \frac{\partial(\eta w)}{\partial \eta} + \frac{\partial f}{\partial \tau} = 0$$

Add on both sides of this equation the term $\frac{\partial}{\partial x}(\eta u)$, then rearrange and end up with:

$$\left.\begin{aligned} &\frac{\partial(\eta u)}{\partial x} + \frac{\partial(\eta w)}{\partial \eta} = \Omega(x, \eta, \tau) \\ &\Omega(x, \eta, \tau) = \eta(1-f)\frac{\partial u}{\partial x} - \frac{\partial f}{\partial \tau} \end{aligned}\right\} \tag{A6a}$$

$$\text{**Integral form:} \quad \int_0^1 u(x, \eta, \tau)\,\eta d\eta = \frac{|f'|}{f}x \tag{A6b}$$

B. Momentum equation

$$\frac{\partial u}{\partial \tau} + u\frac{\partial u}{\partial x} + \frac{1}{f}\left(w + \frac{\partial f}{\partial \tau}\right)\frac{\partial u}{\partial \eta} - \frac{\eta}{f}\frac{\partial u}{\partial \eta}\frac{\partial f}{\partial \tau} = -\frac{\partial p}{\partial x} + \frac{1}{Re}\frac{1}{f^2}\frac{1}{\eta}\frac{\partial}{\partial \eta}\left(\eta\frac{\partial u}{\partial \eta}\right)$$

Add on both sides of this equation $w\frac{\partial u}{\partial \eta} + \frac{1}{Re}\frac{1}{\eta}\frac{\partial}{\partial \eta}\left(\eta\frac{\partial u}{\partial \eta}\right)$, rearrange, and end up with

$$\begin{aligned}\frac{\partial u}{\partial \tau} + u\frac{\partial u}{\partial x} + w\frac{\partial u}{\partial \eta} &= -\frac{\partial p}{\partial x} + \frac{1}{Re}\frac{1}{\eta}\frac{\partial}{\partial \eta}\left(\eta\frac{\partial u}{\partial \eta}\right) + F \\ F(\tau, x, \eta) &= \frac{1-f^2}{f^2}\frac{1}{Re}\frac{1}{\eta}\frac{\partial}{\partial \eta}\left(\eta\frac{\partial u}{\partial \eta}\right) \\ &\quad + \frac{f-1}{f}w\frac{\partial u}{\partial \eta} + \frac{1}{f}(\eta - 1)\frac{\partial u}{\partial \eta}\frac{\partial f}{\partial \tau}.\end{aligned} \tag{A7}$$

In the physical (x, r, τ) coordinate system, the energy equation reads, with $\theta = \frac{T-T_\infty}{T_0-T_\infty}$,

$$\left.\begin{aligned}&\frac{\partial \theta}{\partial \tau} + u\frac{\partial \theta}{\partial x} + w\frac{\partial \theta}{\partial r} = \frac{1}{Re\,Pr}\nabla^2\theta + \frac{Ec}{Re}\varphi \\ &Ec = \frac{V_0^2}{c(T_0 - T_\infty)} \quad \text{and} \quad Pr = \frac{\mu c}{k}\end{aligned}\right\}. \tag{A8}$$

The dimensionless boundary and initial conditions are given in the text.

Concerning the initial conditions, they must be chosen such that the system is not too far from equilibrium solution to avoid numerical instability. It has been observed that a zero initial axial velocity all along the tube does not meet this condition, particularly downstream, owing to the instantaneous growth of the flow rate. Instead, the limit as time goes to zero of the mean flow velocity, Eq. (A3), turned out to be an excellent approximation for the initial axial velocity and resulted in physically realistic results that certify the different validation tests in Section 4.

References

[1] Bejan, A., A study of entropy generation in fundamental convective heat transfer, J. Heat Transfer, 101 (1979), 718–725.

[2] Bejan, A., Entropy Generation Minimization, CRC Press, Boca Raton/New York, 1996.

[3] Mahmud, S., Fraser, R.A., Thermodynamic analysis of flow and heat transfer inside channel with two parallel plates, Exergy, 2 (2002), 140–146.
[4] Mahmud, S., Fraser, R.A., Second law analysis of heat transfer and fluid flow inside a cylindrical annular space, Exergy, 2 (2002), 322–329.
[5] Mahmud, S., Fraser, R.A., The second law analysis in fundamental convective heat transfer problems, Exergy, 42 (2003), 177–186.
[6] Tasnim, S.H., Sohel, M.M., Entropy generation in a porous channel with hydro magnetic effect, Exergy, 2 (2002), 300–308.
[7] Haddad, O., Alkam, M.K., Khaswneh, M.T., Entropy generation due to laminar forced convection in the entrance region of a concentric annulus, Energy, 29 (2004), 35–55.
[8] Lingen, C., Chich, W., Fengrin, S., Finite time thermodynamic optimisation or entropy generation minimisation of energy systems, J. Non-Equilib. Thermodyn., 24 (1999), 327–359.
[9] Michaelides, E.E., Michaelides, E.A., Entropy production, friction factors and holdup in particular two phase flow in pipe, J. Non-Equilib. Thermodyn., 32 (2007), 143–154.
[10] Heil, M., Stokes flows in elastic tube – A large displacement fluid-structure interaction problem, Int. J. Numer. Methods Fluids, 28 (1998), 243–265.
[11] Benyahia, N., Souidi, F., Fluid-structure interaction in pipe flow, Prog. Comput. Fluid Dynam., 6 (2007), 354–362.
[12] Takabateck, S., Ayukawa, K., Numerical study of two-dimensional peristaltic flows, J. Fluid Mech., 12 (1982), 439–465.
[13] Uchida, S., Aoki, H., Unsteady flows in a semi-infinite contracting or expanding pipe, J. Fluid Mech., 82 (1977), 371–387.

Paper received: 2009-01-08
Paper accepted: 2009-03-11